Geophysical Prospecting 35, 236–249, 1987.

MODELING OF SH-WAVE PROPAGATION IN AN IRREGULARLY LAYERED MEDIUM— APPLICATION TO SEISMIC PROFILES NEAR A DOME*

M. CAMPILLO**

ABSTRACT

CAMPILLO, M. 1987, Modeling of SH-Wave Propagation in an Irregularly Layered Medium—Application to Seismic Profiles Near a Dome, Geophysical Prospecting 35, 236–249.

An approach that relies on a discrete representation of seismic wavefields allows the computation of synthetic SH-seismograms in a laterally varying medium with plane and curved interfaces in the two dimensional (2-D) case. The diffracting interface is represented by an array of body forces located along the interface at equal spacing. The numerical treatment is limited to the irregular boundary while the propagation in flat layered zones is obtained by the reflection–transmission matrix method. As an example we have studied the case of a dome in a stratified medium. The solutions obtained verify the reciprocity theorem with good accuracy. The computation of vertical profiles and of surface reflection profiles illustrates the effects of diffraction and the importance of lateral propagation in such a structure.

INTRODUCTION

A stack of flat layers is often a sufficiently accurate model of the structure of the Earth's crust. In such models the discrete wavenumber representation of the seismic field (Bouchon and Aki 1977, Bouchon 1981) is a powerful tool to compute complete seismograms. This method allows the calculation of realistic vertical seismic profiles, including all multiples and conversions (Dietrich and Bouchon 1985a). The models may include attenuating media (Dietrich and Bouchon 1985b) or porous layers (Schmitt, Bouchon and Bonnet 1985). Nevertheless, the effects of lateral heterogeneities have been recognized in actual seismic data both for large scale seismology experiments and for near-surface exploration records. Recently, several authors have improved upon the calculation of synthetic seismograms in laterally

* Received September 1985, last material August 1986.

** Laboratoire de Géophysique Interne et Tectonophysique, Université Scientifique et Médicale de Grenoble, IRIGM, B.P. 68, 38402 Saint-Martin-d'Heres Cedex, France.

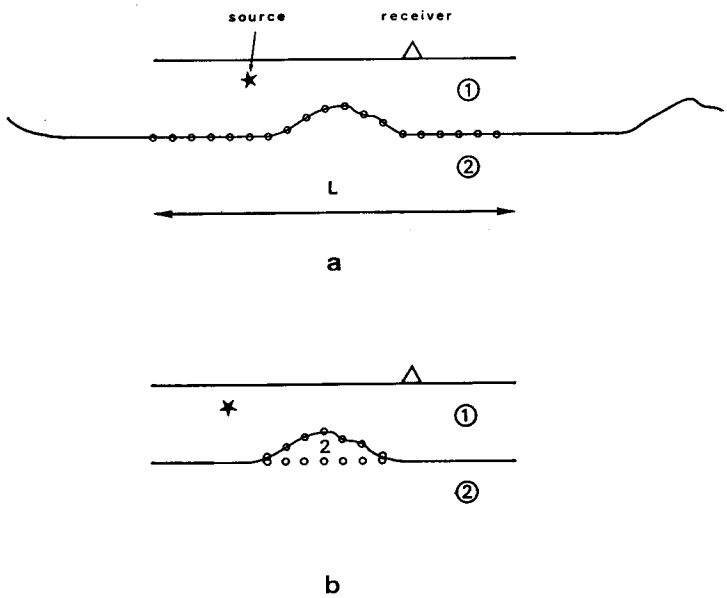

Fig. 1. Geometry of the problem. The medium is assumed to be periodic in x-direction. (a) The interface is discretized at regular spacing on the x-axis in its entire length. (b) The irregular zone is treated as a buried diffractor with a boundary discretized at regular spacing.

varying media—e.g., Haynes (1984a, b, c), Mikhailenko (1984), Červeny and Klimes (1984), Cormier and Spudich (1984), McMechan (1985) and Virieux (1985) have presented realistic computations in complex media. The present work shows the capability of building synthetic SH-seismograms in a 2-D, laterally varying medium by the discrete wavenumber method. Completeness of the solution and the possibility of a realistic representation of the medium are preserved in this extension of the method. The basic principles of the treatment of the irregularities have already been presented for the simplest cases: Bouchon (1985) has computed the response of irregular topographies to incident plane SH-waves while Campillo and Bouchon (1985) have calculated synthetic seismograms in a half-space made up of two media separated by an irregular interface. An improvement of the method is presented allowing the consideration of more complex structures in a more efficient way.

Method of Computation

The basic principles of the method are given by Campillo and Bouchon (1985). They use a discretized form of boundary integral equations. In the case of a buried irregular interface the fields 'reflected' and 'refracted' by the interface are represented by the radiation of arrays of forces distributed along the border at equal spacing (fig. 1a). These distributions are chosen such that the boundary conditions are satisfied. To obtain the strength of each force, one must solve a linear system of

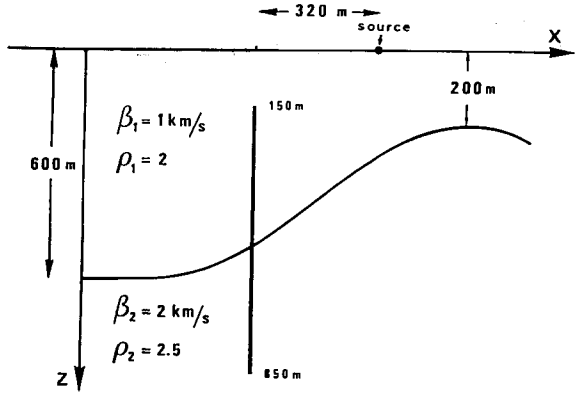

Fig. 2. Source–receiver positions and geometry of the medium used to test the equivalence of the two approaches.

equations given by the boundary conditions and Green's functions of the problem. A well-known problem arises with the singularity of the stress field at the point of application of a force. Approximate solutions have been proposed, e.g., by Kupradze (1963) and applied by Sanchez–Sesma and Esquivel (1979) to a seismological problem. Our approach relies on the discrete wavenumber representation (Bouchon and Aki 1977) to compute the radiation of each source in the frequency domain. The use of truncated Fourier series in place of the actual Green's function eliminates the problem of the stress singularity. The order of truncation of the series depends on the spacial resolution desired (Campillo and Bouchon 1985) which is given in practice by the frequency range considered. The discrete wavenumber method considers a spacial periodicity, L, of sources and medium. In the first formulation of our technique the interface was entirely treated as a diffrator in spite of the limited size of the zone of interest. Then we applied a numerical resolution along the boundary over a length L where the interface could be considered flat in its most important part. This suggests an alternate definition of the diffracting boundary (fig. 1b) in which the model is represented by a flat layered medium with a buried diffracting body. Thus we greatly reduced the dimension of the numerical problem but we needed to use Green's function of the layered half-space. Two techniques of propagation in a stack of flat layers may be envisaged to compute Green's function in the discrete wavenumber context: the matrix propagator method (Harkrider 1964) and the reflection–transmission matrix method (Kennett 1983). The reflection–transmission matrix method is better suited to numerical calculations particularly in the case of evanescent waves. To test the equivalence of the two model representations (fig. 1a and b) we computed synthetic seismograms in a medium consisting of a layer of varying thickness overlying a homogeneous half-space. The geometry of the model is given in fig. 2. This model was also used by Campillo and Bouchon (1985). We compared the results obtained with the same conditions of calculation by considering (i) a complete diffraction interface and (ii) by representing the irregularity as a buried body of finite length in a stratified half-space. The discretization of the

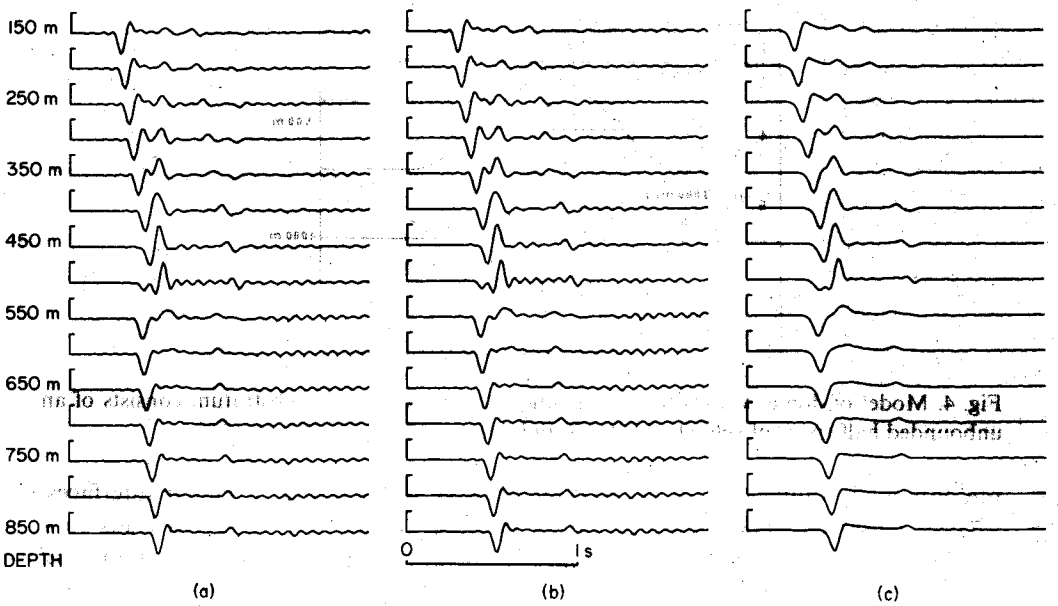

Fig. 3. Synthetic seismograms obtained for the configuration in fig. 2. (a) Results obtained by considering a complete diffracting interface. (b) Results obtained by representing the irregularity by a buried body in a layered half-space. (c) The previous traces after low-pass filtering to eliminate noise.

diffracting boundaries was done at a constant interval along the x-axis, equal to one-half of the shortest wavelength. The source function is

$$S(\omega) = \frac{\omega^2 t_0}{\sinh(\omega\pi t_0/4)},$$

with $t_0 = 0.06$ s. The calculations were done for frequencies between 0 Hz and 16 Hz. The results are shown in fig. 3. The seismograms obtained by the two approaches are identical (fig. 3a and b). Nevertheless, one can observe, in these two cases, a perturbation in the last part of the seismograms. After low-pass filtering (fig. 3c) the noise disappeared. The highest frequency in fig. 3c corresponded to a spacial sampling of the boundary at three points per wavelength. We applied this rule to the computation of the following examples. The discretization of the borders is redefined for each value of the frequency.

Model of Salt Dome

We considered the more complicated model of a salt dome (fig. 4). The dome geometry is defined by an irregular sine-shaped interface. Low velocity material is trapped in the upper part of the dome. The elastic parameters in each layer are given in fig. 4. Such a model, although described by relatively few parameters,

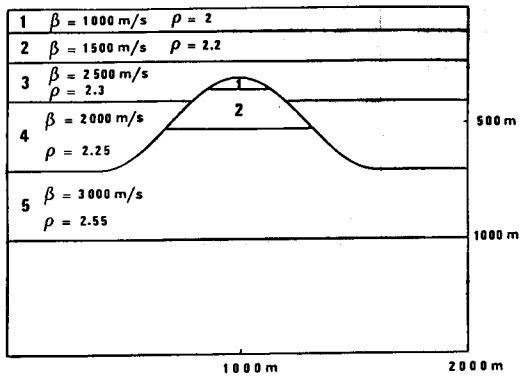

Fig. 4. Model of dome. Velocities and densities are indicated. The substratum consists of an unbounded half-space of velocity 2000 m/s and density 2.25.

presents many difficulties for an analysis of wave propagation: irregular interfaces, wedges, lenses etc. The resolution of the boundary condition equations leads to a solution without any restrictive limitation. As in the previous case the numerical solution is limited to the boundary of the irregular region while the boundary conditions along the flat interfaces are satisfied a priori by the use of Green's functions of the inner and outer stratified media. To test whether the numerical efficiency of the method is affected by factors such as an eventual loss of precision in the computation of Green's functions of the layered media or the discrete representation of the boundaries, we needed a quantitative estimate of the quality of the synthetic seismograms. For this we used a fundamental property of the elastic wavefield—the reciprocity theorem.

Reciprocity

We have tried to compare reciprocal configurations in conditions likely to cause the maximum number of possible errors. Such conditions are present for the configuration displayed in fig. 5. As the salt dome has a symmetrical shape, we expect that

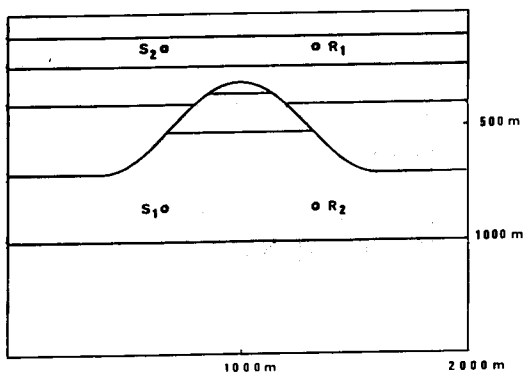

Fig. 5. The reciprocal configuration S_1–R_1 and S_2–R_2.

the displacement produced at R_1 by a force acting at S_1 is equal to the displacement produced at R_2 by a force at S_2. The irregular boundary is discretized in a non-symmetrical manner. The systems of boundary conditions to be solved are completely different for the two calculations. We computed the synthetic seismograms in the frequency range between 0 Hz and 15 Hz. The resulting seismograms are shown in fig. 6. The two traces are very similar except for the later parts. This effect is probably due to the use of a complex frequency in the calculation which required us to remove the effect of the imaginary part of frequency (time damping) by multiplying the time series by an increasing exponential. This operation enhances numerical errors at the end of the seismograms. We also present in fig. 6 the spectral ratio, the coherence and the phase of the cross-spectrum for the two seismograms. The differences between the two seismograms seem to be spread uniformly in the frequency range of the calculation. We conclude from this test that (i) the solution accurately satisfies the reciprocity theorem and (ii), the final part of the time window of calculation is most strongly affected by numerical noise because of the use of a complex frequency for the evaluation of Green's functions and of the source field.

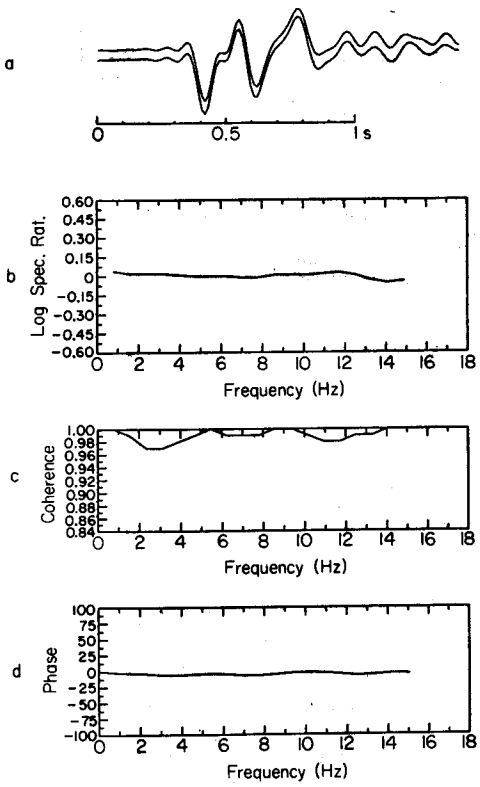

Fig. 6. (a) Reciprocal seismograms corresponding to couples S_1–R_1 and S_2–R_2. (b) Spectral ratio, (c) Coherence between the two traces. (d) Phase of the cross-spectrum of the two signals.

Examples of Simulation of Vertical Seismic Profiles

For the medium geometry and the conditions of calculation of the previous section, we present simulation of vertical seismic profiles on the flank of the dome for different source offsets. Thirty-five receivers are located between 100 m and 850 m depth. The vertical profile is on the right side of the dome at 327 m from its axis of symmetry. Calculations are made for frequencies between 0 Hz and 15 Hz. Figure 7 (a)–(e) presents the results. Three-dimensional plots of the seismograms illustrate the amplitudes of the different phases. The same section is presented after amplitude normalization and use of a saturation of the signal (set to 1/2). Sketches give the

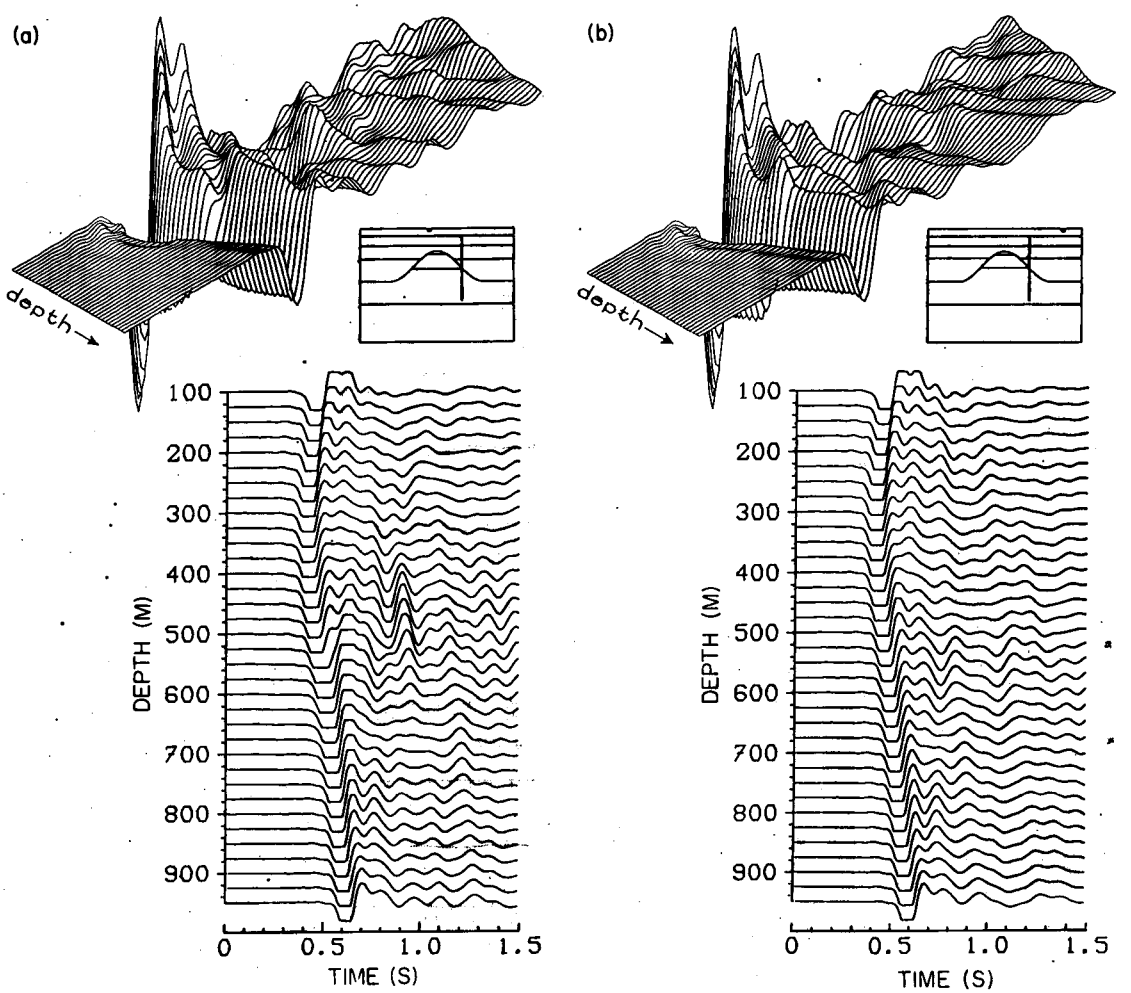

Fig. 7. (a)–(d) Synthetic vertical seismic profiles produced for different source offsets and source depths. The representation is described in the text.

source-receivers configuration. In fig. 7a source and receivers are on opposite sides of the dome. The horizontal offset is 430 m and the source depth is 1 m. The general aspect of the seismograms shows the prominent role played by the first arrival and by the down-going waves. The decay of amplitude with depth is very rapid in spite of our 2-D approach. The amplitude of the first arrival is strongly affected by the scattering over the top of the dome. For depths between 425 m and 525 m, the 3-D representation reveals that the first arrival is weakened by a shadow zone effect because the waves, incident on the low velocity material of the top of the dome, are strongly refracted downwards. This diminution of the true maximum amplitude of the seismograms tends to enhance the importance of the later arrivals on the normalized amplitude section. It is particularly clear with the event appearing at 0.9 s between 400 m and 550 m depth which is due to an interference between up-going and down-going waves.

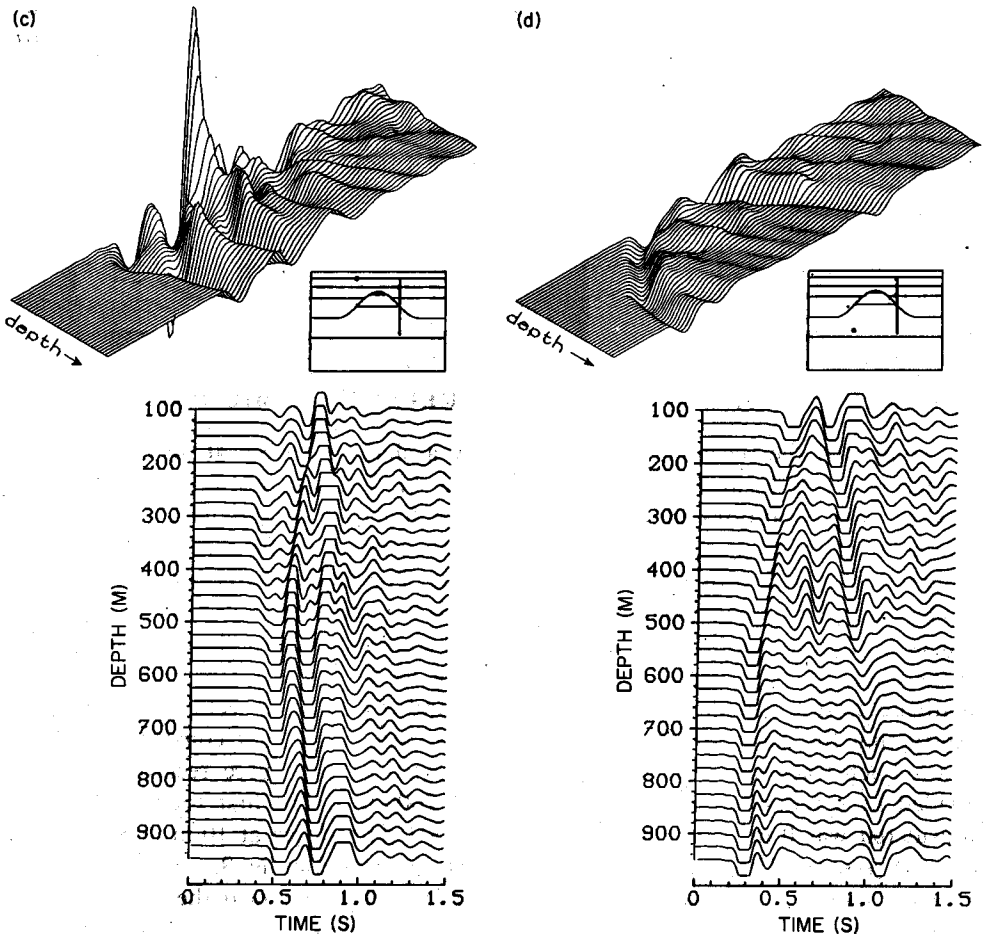

Fig. 7 *Continued*

The reflection on the interface between media 2 and 5 in the dome is clearly visible as an up-going wave which originates at 560 m depth and follows the first arrival. Figure 7b presents the results obtained for the same source offset (430 m) in the opposite direction. Now, the first arrival is no longer affected by a geometrical shadow zone. The internal stratification of the dome is not visible. However, down-going waves in the upper part of the section are stronger because significant energy is reflected by the flank of the dome towards the surface and back to the receiver line. Note the advance of the first arrival on fig. 7b with respect to fig. 7a. In the last case the low velocity materials in the salt dome introduce large time delays in the propagation.

Figure 7c shows an example of computation for a larger offset. The source is now at 100 m depth and at 654 m lateral distance from the receiver line. In this configuration the first arrival at the shallowest receivers consists of head waves. Because the source is at depth the wave shapes are complex. With this large offset the lateral propagation plays a prominent part on the upper half of the section. In the late part of the seismograms, numerous strong reflected phases interact to create involved patterns. The differences in maximum amplitude of the seismograms between the upper and lower part of the profile is greater than in the cases previously presented. With fig. 7d, we considered the case where the structure is illuminated from below. The source offset is still 654 m but the source depth is now 850 m. The amplitudes of the seismograms are quite similar over the whole depth range. A particular effect of the dome structure occurs on the arrival reflected on the discontinuity at 200 m depth: this down-going wave is reflected at a grazing incidence on the flank of the dome and is associated with a strong amplitude.

Examples of Simulation of Surface Seismic Profiles

We computed the seismograms produced by a shallow source at an array of 35 surface receivers located above the dome (fig. 8). The receiver line extends over 1400 m. The conditions of calculation, source function and frequency range are similar to those for previous examples. We concentrated on the comparison of seismograms obtained with and without the dome. The latter model is similar to the model outside the dome (fig. 4), i.e., layer 1–2–3–4–5 and an unbounded substratum. The computations have been done for different source offsets to illustrate the effects of the dome on the different types of waves (fig. 9a–e). We show for each offset the synthetic section calculated for both models and a difference section obtained by subtracting the seismograms of the flat layers case from those computed for the dome. Each trace has been shifted by a time equal to the source–receiver distance divided by a reduction velocity, chosen to be 2000 m/s. The first source offset we considered was 0 m. The source consists in a SH-point-force at 10 m depth below the first receiver. The seismograms obtained are presented in fig. 9a. We can shortly interpret the different phases produced by vertical reflections near the source in the flat-layer model. The numbers i indicated on fig. 9a denote, respectively, the arrivals from the base of the ith layer. The polarity of each phase i is governed by the sign of

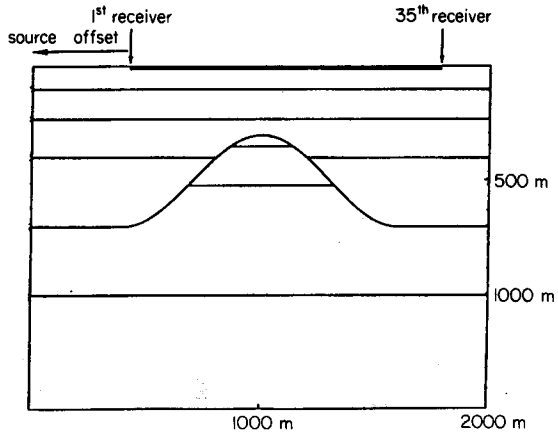

Fig. 8. Receiver–medium configuration for the surface seismic profiles.

the impedance discontinuity between layer i and layer $i + 1$. In the presence of the dome these patterns are perturbed by the waves diffracted on the irregular boundaries. At receivers above the source the difference seismograms show that the perturbations affect reflections 4 and 5. Non-vertical reflections on the flank of the dome are responsible for this discrepancy. At larger distances the perturbations reach reflection 3. Note that the difference traces are effectively zero before the arrival of waves reflected on the irregular structure. The absence of noise is another indication of the accuracy of our calculations. The most spectacular effect of the dome is the appearance of the phase denoted by *d*. This phase is a lateral reflection inside the dome. Because of low velocities in the upper part of the dome, significant energy can be trapped there. This effect of lateral propagation is responsible for the abnormally low apparent velocity of this phase. For flat-layers the first arrival at the furthest receivers is a head wave which propagates horizontally in layer 3. The presence of the dome affects this arrival, although the top of the structure does not reach the interface between layers 2 and 3 but lies 70 m below it. Nevertheless, because of the wavelength of the incident wave (greater than 170 m) the head wave is slightly diffracted by the structure. This is another example of a non-geometrical effect.

Next we considered a source offset of 300 m (fig. 9b). The effect of the dome on the first arrival is striking. As shown by the difference seismograms, the perturbation of the first arrival starts at a distance of about 750 m from the first receiver and corresponds to the head wave which has encountered the dome. The presence of the dome causes a delay of the first arrival and a general distortion of the section before the arrival of the direct wave. This is particularly clear for the phase appearing at about 0.5 s in our time reduced section—this phase loses its rectilinear aspect in the presence of the dome.

Figure 9c presents the results for a source offset of 600 m. We have darkened the negative arches in order to emphasize the beginning of the signals. In the presence of the dome and above its flank opposite to the source (at about 1300 m from the source) the head waves display a complex pattern. At these distances head waves

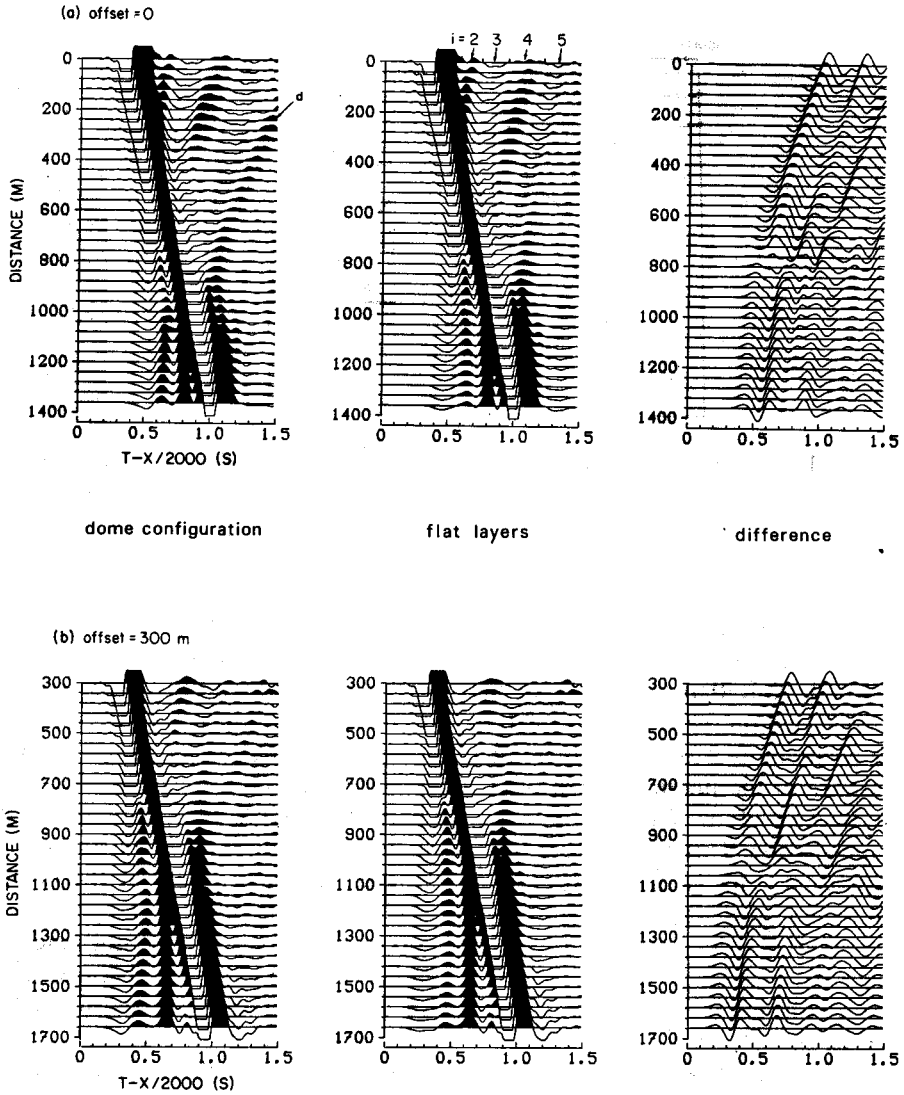

Fig. 9. (a)–(e) Synthetic surface seismic profiles produced for different source offsets. The seismograms have been calculated with and without the dome, and a difference section is shown.

appear propagating in deeper regions (layer 5) which are strongly affected by the presence of the irregular structure.

Finally we placed the source above the dome. Figure 9d shows the results for an offset of -300 m. In the presence of the dome the section loses its symmetry with respect to the source location. The reflections over the flank of the structure are responsible for this effect. The top of the dome is indicated by the rapid decay of amplitude of the reflection over the roof of layer 5, for receivers beyond coordinate

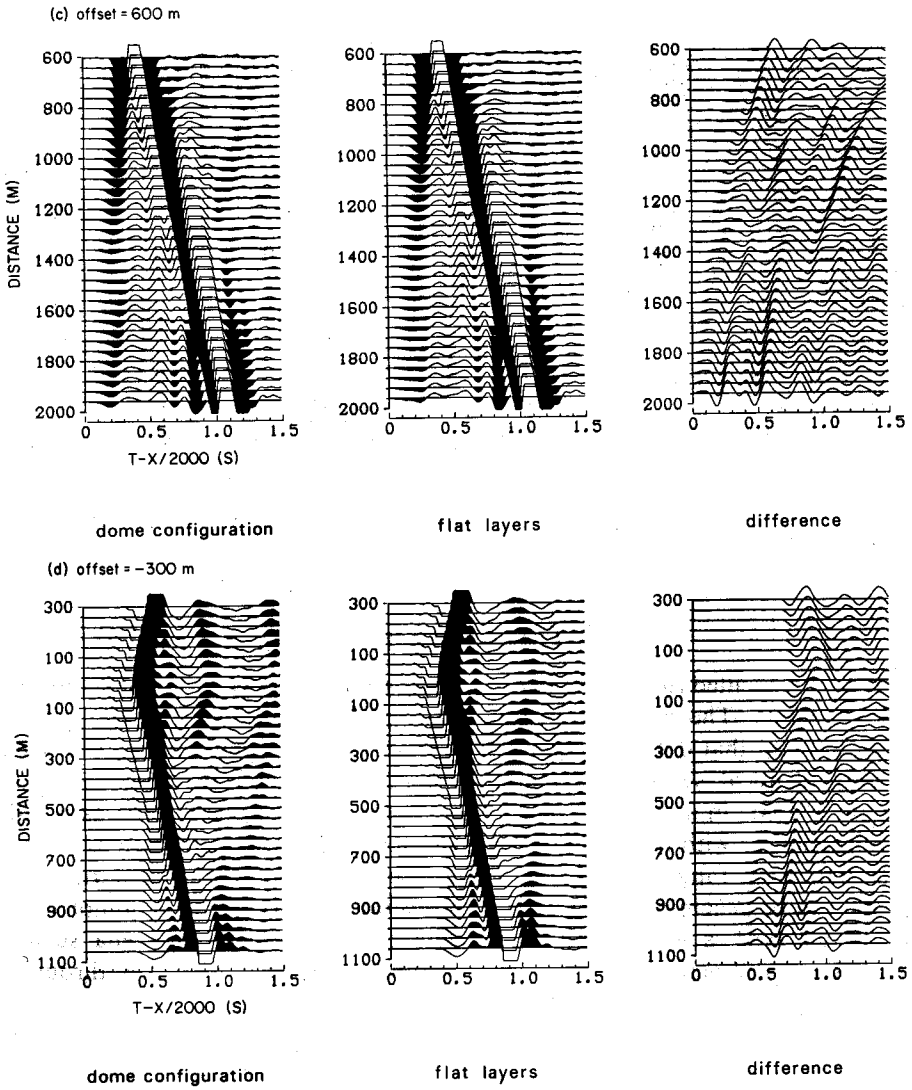

Fig. 9. *Continued*

220 m. This decay is due to the geometry of the low velocity inclusion at the top of the dome which acts as a divergent lens. An important phase is the lateral reflection inside the dome (denoted by *d* in fig. 9a). This phase is also present with a strong amplitude with a source offset of −600 m (fig. 9e), i.e., with the source located 25 m from the axis of symmetry of the dome. A 1-D interpretation of such a profile would lead to an erroneous model. Note the asymmetrical characteristics of the reflection branches, even for the small offset of the source from the axis of the dome.

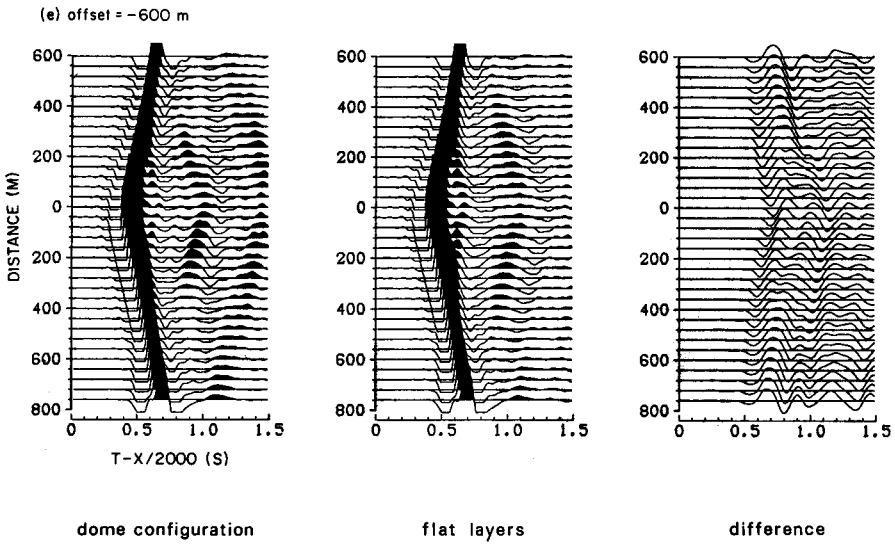

Fig. 9. *Continued*

Conclusion

The method presented allows the realistic simulation of the wave propagation in a complex medium. The numerical solution can be limited to the irregularity itself. We have verified that different numerical representations of the same problem lead to exactly identical solutions. Reciprocity holds with good precision. We have shown for a dome in a stratified medium some examples of phenomena associated with diffraction or with reflection on irregular structures. The method does not rely on the frequency range considered nor on the shape of the irregularity. This approach can be generalized for media with several heterogeneities. A complete solution of this type is well suited to simulate quantitatively phenomena such as shadow zones, diffraction by a wedge, or propagation of head waves through a complex medium.

Acknowledgments

I thank Michel Bouchon for his help during the study. This work was supported by the Centre de Calcul Vectoriel pour la Recherche and by the Département Sismique de Puits, Societé Nationale Elf Aquitaine (Production).

References

Bouchon, M. 1981, A simple method to calculate Green's functions for elastic layered media, Bulletin of the Seismological Society of America 71, 959–971.

Bouchon, M. 1985, A simple, complete numerical solution to the problem of diffraction of SH waves by an irregular surface, Journal of the Acoustic Society of America 20, 1–5.

BOUCHON, M. and AKI, K. 1977, Discrete wavenumber representation of seismic source wavefields, Bulletin of the Seismological Society of America 67, 259–271.

CAMPILLO, M. and BOUCHON, M. 1985, Synthetic SH-seismograms in a laterally varying medium by the discrete wavenumber method, Geophysical Journal of the Royal Astronomical Society 82, 307–317.

ČERVENY, V.L. and KLIMES, L. 1984, Synthetic body wave seismograms for three dimensional laterally varying media, Geophysical Journal of the Royal Astronomical Society 79, 119–133.

CORMIER, V.F. and SPUDICH, P. 1984, Amplification of ground motion and waveform complexity in fault zones: examples from the San Andreas and Calaveras faults, Geophysical Journal of the Royal Astronomical Society 79, 135–152.

DIETRICH, M. and BOUCHON, M. 1985a, Synthetic vertical seismic profiles in elastic media, Geophysics 50, 224–234.

DIETRICH, M. and BOUCHON, M. 1985b, Measurement of attenuation from vertical seismic profiles by iterative modeling, Geophysics 50, 931–949.

HARKRIDER, D.G. 1964, Surface waves in multilayered elastic media, Part I: Rayleigh and Love waves from buried sources in a multilayered half-space, Bulletin of the Seismological Society of America 54, 627–680.

HAYNES, A.J. 1984a, A phase-front method I: narrow frequency band SH waves, Geophysical Journal of the Royal Astronomical Society 72, 783–808.

HAYNES, A.J. 1984b, A phase-front method II: broad frequency band SH waves, Geophysical Journal of the Astronomical Society 77, 43–64.

HAYNES, A.J. 1984c, A phase-front method III: acoustic waves, P- and S-waves, Geophysical Journal of the Royal Astronomical Society 77, 65–103.

KENNETT, B.L.N. 1983, Seismic Wave Propagation in Stratified Media, Cambridge University Press.

KUPRADZE, V.D. 1963, Dynamical problems in elasticity *in* Progress in Solid Mechanics, 3, I.N. Sneddon and R. Hill (eds), North Holland Publishing Company.

MCMECHAN, G.A. 1985, Synthetic finite-offset vertical seismic profiles for laterally varying media, Geophysics 50, 627–636.

MIKHAILENKO, B.G. 1984, Synthetic seismograms for complex three-dimensional geometries using an analytical-numerical algorithm, Geophysical Journal of the Royal Astronomical Society 79, 963–986.

SANCHEZ-SESMA, F.J. and ESQUIVEL, J.A. 1979, Ground motion on alluvial valleys under incident plane SH-waves, Bulletin of the Seismological Society of America 69, 1107–1120.

SCHMITT, D.P., BOUCHON, M. and BONNETT, G. 1987, Full wave synthetic acoustic logs in saturated porous media, submitted to Geophysics.

VIRIEUX, J. 1985, SH-wave propagation in heterogeneous media: velocity stress finite difference method, Geophysics 49, 1933–1957.